JOURNAL OF GEOPHYSICAL RESEARCH, VOL. 112, F02013, doi:10.1029/2005JF000402, 2007

Integration of geochemical mass balance with sediment transport to calculate rates of soil chemical weathering and transport on hillslopes

Kyungsoo Yoo,[1,2] Ronald Amundson,[1] Arjun M. Heimsath,[3] William E. Dietrich,[4] and George H. Brimhall[4]

Received 31 August 2005; revised 30 September 2006; accepted 10 November 2006; published 9 May 2007.

[1] We developed a process-oriented hillslope soil mass balance model that integrates chemical and physical processes within hillslope soils. The model explicitly factors that soil chemical weathering at any hillslope position is related to the flux of soil eroded from upslope as well as soil production from underlying bedrock. The model was merged with measurements of soil elemental chemistry and cosmogenic radionuclide-based saprolite-to-soil conversion rates along a 50 m transect of a semiarid granodiorite hillslope in the southeastern Australian highlands. Inverse modeling results in the simultaneous quantification of the rates of soil chemical weathering and soil transport as a function of hillslope position. Soil chemical weathering rates per land surface area systematically varied along the transect from losses of 0.035 kg m^{-2} yr^{-1} on the ridge to gains of 0.035 kg m^{-2} yr^{-1} at the lowest slope position. The mass loss via soil chemical weathering would have been overestimated by 40% if the impact of soil transport on soil chemistry was ignored. The chemical mobility of elements, combined with biological nutrient demand, controlled the spatial redistribution of individual elements: P and Ca were preferentially retained relative to Si, Al, and Fe within the hillslope base. The calculated soil transport rate is linearly related to the product of soil thickness and slope gradient, instead of slope alone. Soil residence time was determined by calculating the time length for a 3 dimensional box (volume = 1 m^2 surface area $\times$ soil thickness) to be entirely removed by mass flux of soil transport: 4 ka on the ridge to 0.9 ka at the hillslope base. These soil residence times, combined with soil chemical weathering rates, indicate that a 1 m^2 area of soil loses $\sim$1,800 kg via chemical weathering while passing through the upslope portion of the hillslope, but that it regains $\sim$90 kg, probably via clay precipitation and biological retention of cations, during its passage through the lower segments of the transect. This study provides a previously unrecognized linkage between physical soil transport and soil chemical weathering that have implications for hillslope evolution as well as biogeochemistry.

Citation: Yoo, K., R. Amundson, A. M. Heimsath, W. E. Dietrich, and G. H. Brimhall (2007), Integration of geochemical mass balance with sediment transport to calculate rates of soil chemical weathering and transport on hillslopes, *J. Geophys. Res.*, *112*, F02013, doi:10.1029/2005JF000402.

1. Introduction

[2] Soil chemical weathering, together with physical generation and transport of sediment (hereafter soil), helps shape the earth's surface. The chemical weathering of the earth's surface forms soils [*Amundson*, 2004], controls the chemistry of stream water [*Likens and Bormann*, 1977], sustains ecosystem productivity [*Porder et al.*, 2005], contributes to the morphologic evolution of landscapes [*Mudd and Furbish*, 2004], and modulates atmospheric CO_2 levels on geological timescales [*Berner*, 1995]. Recent efforts have determined how weathering rates respond to climate [*Riebe et al.*, 2004; *White and Blum*, 1995], vegetation [*Berner and Berner*, 2004; *Drever*, 1994], mineralogy [*Brantley and Chen*, 1995], time [*White et al.*, 1996], and tectonic uplift [*Riebe et al.*, 2001].

[3] Most soil-based studies of chemical weathering rates focus on nearly level landscapes, where physical soil erosion is minimal and water flux is less complicated, and where the mass loss divided by the geomorphic surface age

[1]Division of Ecosystem Sciences, University of California, Berkeley, California, USA.
[2]Now at Plant and Soil Sciences Department, University of Delaware, Newark, Delaware, USA.
[3]Department of Earth Sciences, Dartmouth College, Hanover, New Hampshire, USA.
[4]Department of Earth and Planetary Science, University of California, Berkeley, California, USA.

0148-0227/07/2005JF000402$09.00

provides the long-term soil chemical weathering rate [e.g., *Chadwick et al.*, 1990; *White et al.*, 1996]. On level landforms, chemical weathering losses can be large enough to significantly affect the elevation of the land surface during soil formation [e.g., *Brimhall et al.*, 1991; *Chadwick et al.*, 1990]. Soil chemical weathering, however, must also occur on sloping terrains. Numerous stream chemistry studies of upland watersheds have shown that chemical weathering contributes to landscape denudation [e.g., *White and Blum*, 1995]. Only recently, however, have soil-based measurements of long-term chemical weathering rates been made on actively eroding landscapes [*Anderson et al.*, 2002; *Riebe et al.*, 2003a, 2003b, 2004]. In particular, *Riebe et al.* [2001, 2003a, 2003b, 2004] developed the principles to determine the catchment-scale relationship between soil chemical weathering rate and mineral supply rate from bedrock (often called soil production rate) by integrating geochemical analyses of soils and bedrock with cosmogenic nuclide analyses of stream sediments.

[4] The spatial variation of soil chemical weathering rates within an eroding hillslope is still largely unknown. Toposequence soil studies, however, repeatedly suggested a systematic variation of soil chemical weathering rates [*Birkeland*, 1999], and more quantitative work is now devoted to understanding the topographic patterns in soil chemical weathering rate [*Nezat et al.*, 2004]. On a more general theoretical front, *Mudd and Furbish* [2004] conducted a mathematical modeling demonstrating that the spatial distribution of soil chemical weathering rates may contribute to the morphologic evolution of a hillslope.

[5] The fundamental starting point in considering a general mass balance of hillslope soils is that weathering occurs in materials derived from in situ bedrock as well as in materials eroded from upslope. Thus the mineral supply for chemical weathering must incorporate both soil production (from rock) and soil transport (from upslope). This paper thus achieves three objectives. First, we develop a soil chemical weathering model that mechanistically combines models of geochemical mass balance [*Brimhall and Dietrich*, 1987] and hillslope soil production and transport [*Dietrich et al.*, 1995; *Heimsath et al.*, 1997]. The resulting model is a general framework that incorporates, as a special case, the method of *Riebe et al.* [2001, 2003a, 2003b, 2004] to link soil chemical weathering to soil production in mountainous uplands. Second, we combine our model with empirical data from a watershed in southeastern Australia to show how the model can be used for simultaneously quantifying the rates of chemical weathering and soil transport as a function of hillslope position. Third, we reassess the current understanding of chemical weathering contributions to hillslope mass removal, and offer some new theoretical insights into hillslope soil formation.

2. Background: Current Models of Soil Chemical Weathering and Transport

[6] We briefly review the current models of soil chemical weathering and transport on eroding landscapes. *Riebe et al.* [2001, 2003a, 2003b, 2004] formulated a soil mass balance expression for the steady state case where soil production is balanced by mass removal via soil erosion and chemical weathering. In this case, $\Phi = E + W$, where Φ is soil production rate from saprolite (or bedrock if saprolite is not present), E is physical soil erosion rate, and W is soil chemical weathering rate (all of the terms have the unit of mass per area per time). In nature, this mass balance can be constrained using immobile elements, such as zirconium, whose mass is controlled only by the physical processes of soil production and erosion: $C_{ip}\Phi = C_{is}E$ where C_i is the concentration of the immobile elements [M M^{-1}], and subscript p and s represent saprolite and soil, respectively. These equations assume that soil mass and composition do not change over time. By solving these two mass balance equations for W, *Riebe et al.* [2001, 2003a, 2003b, 2004] related the soil chemical weathering rate to the soil production rate as

$$W = \left(1 - \frac{C_{ip}}{C_{is}}\right)\Phi, \tag{1}$$

or

$$\mathrm{CDF} = \frac{W}{\Phi} = \left(1 - \frac{C_{ip}}{C_{is}}\right), \tag{2}$$

where chemical depletion factor (CDF) represents the relative contribution of soil chemical weathering in the removal of soil produced from bedrock. This formulation allowed *Riebe et al.* [2001, 2003a, 2003b, 2004] to determine the long-term soil chemical weathering rates by measuring the elemental chemistry of soils versus saprolite and by determining catchment-wide soil production rates using cosmogenic radionuclides in sediments.

[7] While soil chemical weathering rates have not been functionally linked to topographic position, mathematical relationships between soil transport and topography have been actively pursued in geomorphology since *Gilbert*'s [1909] analysis of soil mantled hillslope [*Dietrich et al.*, 2003]. The most widely used slope-dependent soil transport model states that soil flux is linearly proportional to the slope gradient ($-\nabla Z$, where Z is the elevation of ground surface):

$$\tilde{Q}_s = \rho K(-\nabla Z), \tag{3}$$

where $\tilde{Q}_s$ is soil flux [$ML^{-1}T^{-1}$], ρ is soil bulk density [M L^{-3}], and K is a constant commonly called diffusivity [L^2T^{-1}] [*Culling*, 1963]. This linear approximation may not occur everywhere. For example, soil transport becomes nonlinear with increasing slope gradient due to the balance of gravity and friction [*Andrews and Bucknam*, 1987; *Roering et al.*, 1999]. Additionally, it has been repeatedly proposed that soil transport is proportional to the product of soil thickness and slope gradient [*Ahnert*, 1967; *Furbish*, 2003, *Braun et al.*, 2001, *Heimsath et al.*, 2005b]:

$$\tilde{Q}_s = \rho kh(-\nabla Z), \tag{4}$$

where k is a constant [$L\ T^{-1}$] and h is soil thickness [L].

3. Model Development

3.1. Soil Chemical Weathering Rate in Relation to Soil Production and Transport

[8] Soil mass balance expressions were developed separately for bulk soils, a mobile element j, and an immobile

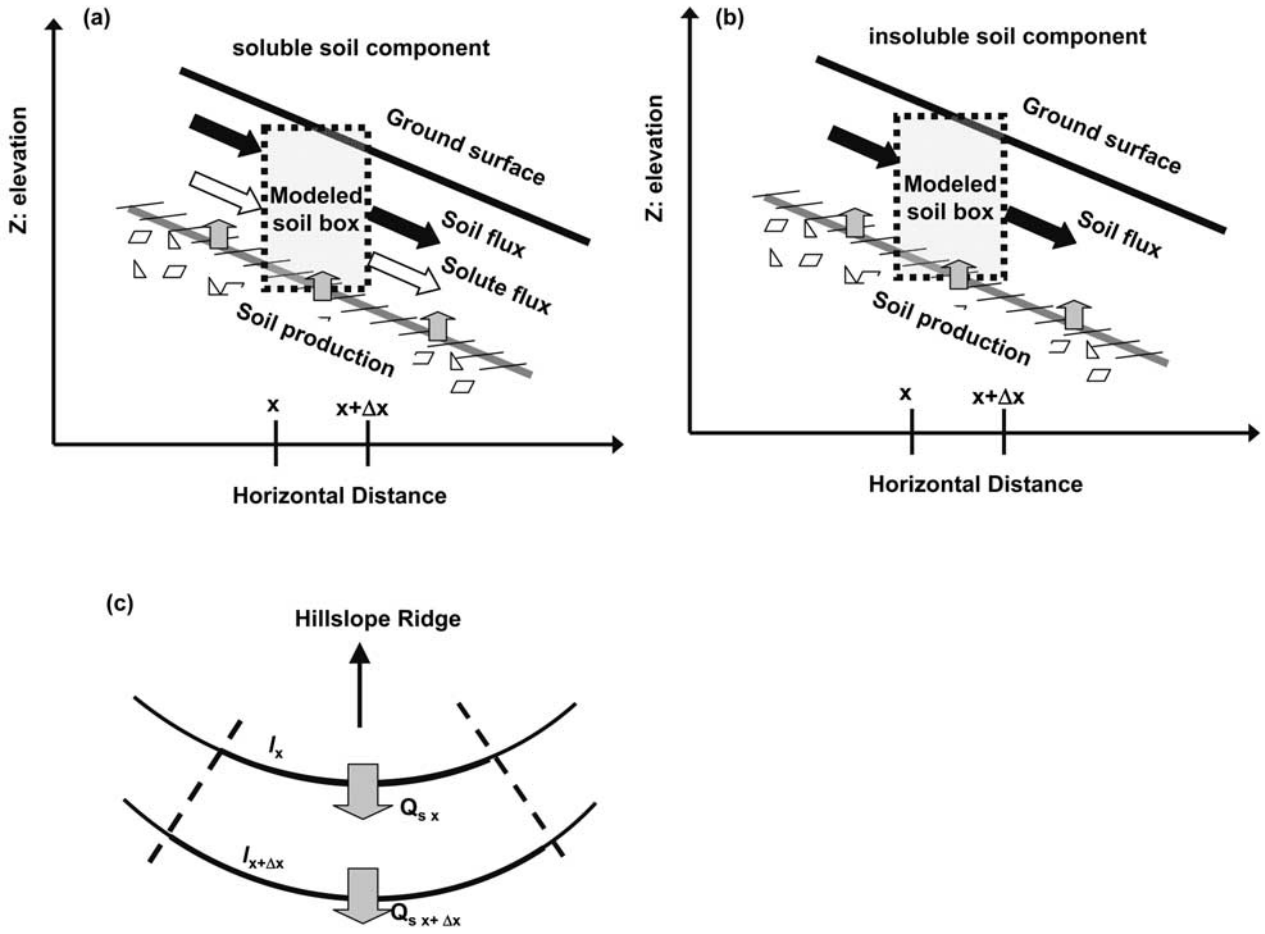

Figure 1. Mass fluxes on hillslope soils: (a) mass fluxes of soluble soil components in and out of a modeled soil box, (b) mass fluxes of an insoluble soil component in and out of a modeled soil box, and (c) plan view of physical sediment flux. In Figure 1c, the sediment flux crossing the lower contour line ($Q_{s\,x+\Delta x} l_{x+\Delta x}$) is equal to the sum of sediment input through the upper contour line ($Q_{s\,x} l_x$) and the excess of soil production rate minus weathering loss rate between the contour lines.

element i. Soil is defined as a mobile layer where biological and physical disturbance of mineral and organic matter leads to downslope-directed mass movement. The mass of any soil component at a given hillslope position is determined by the balance of soil production, sediment flux, and solute flux (Figure 1a). In the case of an immobile (chemically inert) element, the solute flux term is 0 (Figure 1b). The fluxes of both soil and solutes are defined as the mass of material crossing a unit length of a contour line per unit time [$ML^{-1}T^{-1}$]. The divergence of solute and soil fluxes result in the value of the soil chemical weathering rate and the physical soil erosion rate, respectively. The mass conservation equations for a soil box illustrated in Figures 1a and 1b are

$$\frac{\partial(\rho h)}{\partial t} = \Phi - \nabla \cdot \tilde{Q}_S - \nabla \cdot \tilde{Q}_W, \tag{5}$$

$$\frac{\partial(C_{js}\rho h)}{\partial t} = C_{jp}\Phi - \nabla \cdot (C_{js}\tilde{Q}_S) - \nabla \cdot \tilde{Q}_{Wj}, \tag{6}$$

and

$$\frac{\partial(C_{is}\rho h)}{\partial t} = C_{ip}\Phi - \nabla \cdot (C_{is}\tilde{Q}_s), \tag{7}$$

where ρ is soil bulk density [ML^{-3}], h is soil thickness [L], Φ is soil mass production rate [$ML^{-2}T^{-1}$], $\tilde{Q}_s$ is soil flux [$ML^{-1}T^{-1}$], $\nabla \cdot \tilde{Q}_s$ is soil erosion rate [$ML^{-2}T^{-1}$], $\tilde{Q}_w$ is solute flux [$ML^{-1}T^{-1}$], $\nabla \cdot \tilde{Q}_w$ is chemical weathering rate [$ML^{-2}T^{-1}$], C is concentration [MM^{-1}], subscript p and s represent saprolite and soil, respectively, and the subscripts j and i represent mobile and immobile elements, respectively.

[9] If the rates of soil transport, soil production, and chemical weathering are balanced such that the thickness and chemical composition of the soil do not change over time, equations (5) to (7) can be solved for the total and elemental soil chemical weathering rates (for derivation, see Appendix A). As we illustrate later in the results, our analysis concerns a timescale comparable to the soil residence time, which is estimated in this paper to be less than 10 ka at our study site. Given that 100 ka to 1 Ma, timescales much longer than soil residence times, are required for establishing steady state hillslope morphology

[*Fernandes and Dietrich*, 1997; *Roering et al.*, 2001], our assumption of constant hillslope morphology seems reasonable. The expressions for weathering rates are

$$W = \nabla \cdot \tilde{Q}_W = \underbrace{\left(1 - \frac{C_{ip}}{C_{is}}\right)\Phi}_{W_\Phi} + \underbrace{\frac{\nabla C_{is}}{C_{is}} \cdot \tilde{Q}_S}_{W_S}, \quad (8)$$

and

$$W_j = \nabla \cdot \tilde{Q}_{Wj} = \left(1 - \frac{C_{ip}}{C_{is}}\frac{C_{js}}{C_{jp}}\right)(C_{jp}\Phi) + \left(\frac{\nabla C_{is}}{C_{is}} - \frac{\nabla C_{js}}{C_{js}}\right) \cdot (C_{js}\tilde{Q}_S), \quad (9)$$

where W is the weathering loss (positive) or gain (negative) rate [$ML^{-2}T^{-1}$], W_Φ and W_S are used to represent the first and second terms in equation (8), respectively. If sediment flux or the spatial variation of soil chemistry is negligible, the weathering models converge to that of *Riebe et al.* [2001, 2003a, 2003b, 2004] (equation (1)). The first terms represent the role of soil production on soil thickness and chemistry. The second terms, which have not been derived before, describe the role of soil transport on soil thickness and chemistry. Alternatively, the new mass balance model, functionally relates the chemical weathering rate to the mineral supply rates from not only from the underlying saprolite [*Riebe et al.*, 2001, 2003a, 2003b, 2004] but also from the soils upslope.

[10] The soil transport rate must be constrained in the application of the model (Figure 1c). For a sequence of hillslope soils at steady state (Figure 1c), the soil flux at a distance $x + \Delta x$ from ridge is the sum of the soil input at x and the excess of the soil production rate from saprolite, minus the chemical weathering rate, over distance Δx:

$$\left|\tilde{Q}_s\right|_{x+\Delta x} = \int_x^{x+\Delta x} (\Phi - W)dx + \frac{l_x}{l_{x+\Delta x}}\left|\tilde{Q}_s\right|_x, \quad (10)$$

where l is the length of a contour line bounded by two water flow lines (Figure 1c), which makes the calculation scale-dependent. The ratio of the lengths ($l_x/l_{x+\Delta x}$) is 1 on planar slopes and is less than 1 on divergent slopes as in Figure 1c. It is assumed that the soil transport rate is zero at the hillslope divide.

[11] By measuring the soil mass production rate and the elemental chemistry of soils and saprolite along a hillslope transect, we can simultaneously calculate the rates of soil chemical weathering and transport through an iterative process. An arbitrary value is initially made for the soil flux in equation (8). This arbitrary number could be the soil flux obtained by integrating the upslope soil production rates assuming no chemical loss. Regardless of the choice of the initial value of soil flux, however, equations (8), (9), and (10) lead to unique values of soil chemical weathering rate and soil flux. We note that no assumption was made for the mathematical forms (such as equations (3) and (4)) of the soil transport. Then the resulting W is inserted into equation (10), and this process is repeated until W *and* Q_s do not change further. The same procedure is used for calculating the elemental weathering rate (equation (9)).

[12] The results will be used to determine the relative importance of chemical weathering versus physical erosion in removing mass on hillslopes. To do so, we divided the soil chemical weathering rate (equation (8)) by the soil production rate and defined the ratio as the extended chemical depletion factor (ECDF), following the concept of the CDF (equation (2)) as defined by *Riebe et al.* [2003a, 2003b, 2004].

$$ECDF = \frac{W}{\Phi} = \underbrace{\left(1 - \frac{C_{ip}}{C_{is}}\right)}_{\text{CDF(Eq.2)}} + \underbrace{\frac{\nabla C_{is}}{C_{is}} \cdot \frac{\tilde{Q}_S}{\Phi}}_{\substack{\text{Deviation from CDF} \\ \text{due to sediment transport}}}. \quad (11)$$

[13] ECDF differs from CDF (equation (2)) because it includes the effects of physical soil transport on the immobile elemental concentration of soil material. Depending on the sign of ∇C_{is}, ECDF could be larger or smaller than CDF. When the soil chemistry does not vary over a hillslope, an unlikely scenario for most landscapes, the ECDF equals the CDF. Below we show that these two measures are seldom equal at our field site.

3.2. Soil Chemical Weathering in Relation to Soil Residence Time

[14] On nonsloping topography, the soil chemical weathering rate is determined by dividing the mass loss during soil formation, $\Delta_\uparrow$ [ML^{-2}], by soil age, which is equivalent to the age of the geomorphic surface, or the time since erosion or deposition ceased [e.g., *Chadwick et al.*, 1990; *Chadwick et al.*, 1999; *Merritts et al.*, 1991; *White et al.*, 1996]:

$$W = \frac{\Delta_\uparrow}{T_G}, . \quad (12)$$

where T_G = age of geomorphic surface, and $\Delta_\uparrow$, following *Brimhall and Dietrich* [1987], can be defined as (see Appendix B for derivation)

$$\Delta_\uparrow = \left(\frac{C_{is}}{C_{ip}} - 1\right)\rho_s h_s. \quad (13)$$

The concept of 'age of the geomorphic surface', however, is hard to apply to actively eroding landscapes. Below, we argue that the measure of soil residence time is the more relevant parameter on eroding hillslopes and that our new soil weathering equations (equations (8) and (9)) link hillslope soil chemistry to the soil residence time.

[15] Previously, soil residence time on hillslopes has been obtained by dividing soil mass by the soil production rate [e.g., *Heimsath et al.*, 2001], assuming that the soil production rate equals the soil erosion rate (E) that physically removes the soil mass. This assumption is not valid where significant mass loss occurs via chemical weathering. However, the physical erosion rate of an immobile element should be equal to the input rate of the immobile element via soil production such that $C_{is}E = C_{ip}\Phi$ regardless of mass loss via chemical weathering. Accordingly, we can then define soil residence time ($T_{R\uparrow}$) as the time required for the soil Zr mass within a 3 dimensional box (operationally

defined by 1 m^2 surface area and soil thickness) to be replaced by Zr input rate via soil production.

$$T_{R\uparrow} = \frac{\rho_s h_s}{E} = \frac{\rho_s C_{is} h_s}{C_{is} E} = \frac{\rho_s C_{is} h_s}{C_{ip} \Phi}. \quad (14)$$

[16] For a soil located on a hillslope summit, where soil transport from upslope can be ignored, the mass loss via chemical weathering described in equation (13) occurs during the time interval defined in equation (14). In other words, the soil chemical weathering rate can be obtained by dividing the mass loss via chemical weathering (equation (13)) by the soil residence time (equation (14)):

$$\frac{\Delta_\uparrow}{T_{R\uparrow}} = \left(1 - \frac{C_{ip}}{C_{is}}\right)\Phi. \quad (15)$$

Equation (15) is identical to W_Φ in equation (8). However, the weathering rate is now linked to the soil residence time.

[17] We have just shown how to relate W_Φ in equation (8) [*Riebe et al.*, 2001, 2003a, 2003b, 2004] to soil residence time. We can also do the same for W_S to introduce residence time driven by lateral mass fluxes (soil and solute flux from upslope or downslope). From the perspective of a soil on a hillslope position (a soil mass in Figure 1a), a soil located upslope by Δx also serves as a parent material. Thus we can modify equations (13) and (14) to incorporate the influxes from the soil located upslope at Δx in order to calculate the chemical weathering mass loss ($\Delta_\rightarrow$) over distance Δx and the soil residence time ($T_{R\rightarrow}$) which is associated with that transport:

$$\Delta_\rightarrow = \rho_s h \left(\frac{C_{is\_x+\Delta x}}{C_{is\_x}} - 1\right), \quad (16)$$

and

$$T_{R\rightarrow} = \frac{\rho_s C_{is\_x+\Delta x} h \Delta x}{C_{is\_x} Q_{s\_x}}. \quad (17)$$

[18] The chemical weathering rate during lateral soil transport can be calculated by dividing the mass loss via chemical weathering (equation (16)) by soil transport associated soil residence time (equation (17)), which produces the W_S term in equation (8).

$$\frac{\Delta_\rightarrow}{T_{R\rightarrow}} = \frac{C_{is\_x+\Delta x} - C_{is\_x}}{C_{is\_x}} \frac{C_{is\_x} Q_{s\_x}}{C_{is\_x+\Delta x} \Delta x} \quad (18a)$$

$$= \frac{1}{C_{is\_x+\Delta x}} \frac{C_{is\_x+\Delta x} - C_{is\_x}}{\Delta x} Q_{s\_x} \quad (18b)$$

as Δx approaches zero,

$$\equiv \frac{1}{C_{is}} \nabla C_{is} \cdot \tilde{Q}_s = W_S. \quad (18c)$$

We now have presented two distinct soil residence times that (1) differ from previous estimates of residence time on hillslopes, but (2) which explicitly reflect the mass movement of the largely vertical physical soil production and the largely lateral soil fluxes.

[19] Our next task is to combine these two soil residence times to arrive at a total soil residence time (T_{Rt}) which is defined as the time required to remove the materials in a soil box (in Figures 1a and 1b) via soil transport out of the box:

$$T_{Rt} = \frac{\rho h \Delta x}{Q_{s\_x+\Delta x}}. \quad (19)$$

By focusing on an immobile element, as discussed above, we can accurately arrive at residence times without ignoring chemical weathering losses. Note that, in the following equations, the out flux of the immobile element via the soil transport at x + Δx is equal to the input rates of the immobile element via soil production over the distance of Δx and soil transport at x because of the negligible solute flux of the immobile element (Figure 1b).

$$T_{Rt} = \frac{\rho h \Delta x}{Q_{s\_x+\Delta x}} \quad (20a)$$

$$= \frac{\rho C_{is\_x+\Delta x} h \Delta x}{C_{is\_x+\Delta x} Q_{s\_x+\Delta x}} \quad (20b)$$

$$= \frac{\rho C_{is\_x+\Delta x} h \Delta x}{C_{ip} \Phi \Delta x + C_{is\_x} Q_{s\_x}} \quad (20c)$$

$$= \frac{1}{(C_{ip}\Phi)/(\rho C_{is\_x+\Delta x} h) + (C_{is\_x} Q_{s\_x})/(\rho C_{is\_x+\Delta x} h \Delta x)} \quad (20d)$$

$$= \frac{1}{1/T_{R\uparrow} + 1/T_{R\rightarrow}} = \frac{T_{R\rightarrow} T_{R\uparrow}}{T_{R\rightarrow} + T_{R\uparrow}}. \quad (20e)$$

From a geochemical and pedological view, total residence time is clearly an important value. However, knowledge of the two components of this total residence time (equation (20d)) is of considerable importance because it shows that the total soil residence time is largely determined by the greater of the two mass fluxes (soil production rate versus soil transport rate) whose relative significance changes with the soil's position on a hillslope.

[20] The integrated soil residence time can be combined with the soil chemical weathering rate to calculate the mass loss or gain per 1 m length of contour line (ΔM: ML^{-1}) as soil moves from point α to point β along a hillslope transect:

$$\Delta M = \int_\alpha^\beta W \times T_{Rt}\, dx. \quad (21)$$

4. Methods

4.1. Study Site

[21] The research was conducted at Frog's Hollow (FH), a semiarid eucalyptus grassland savannah hillslope located

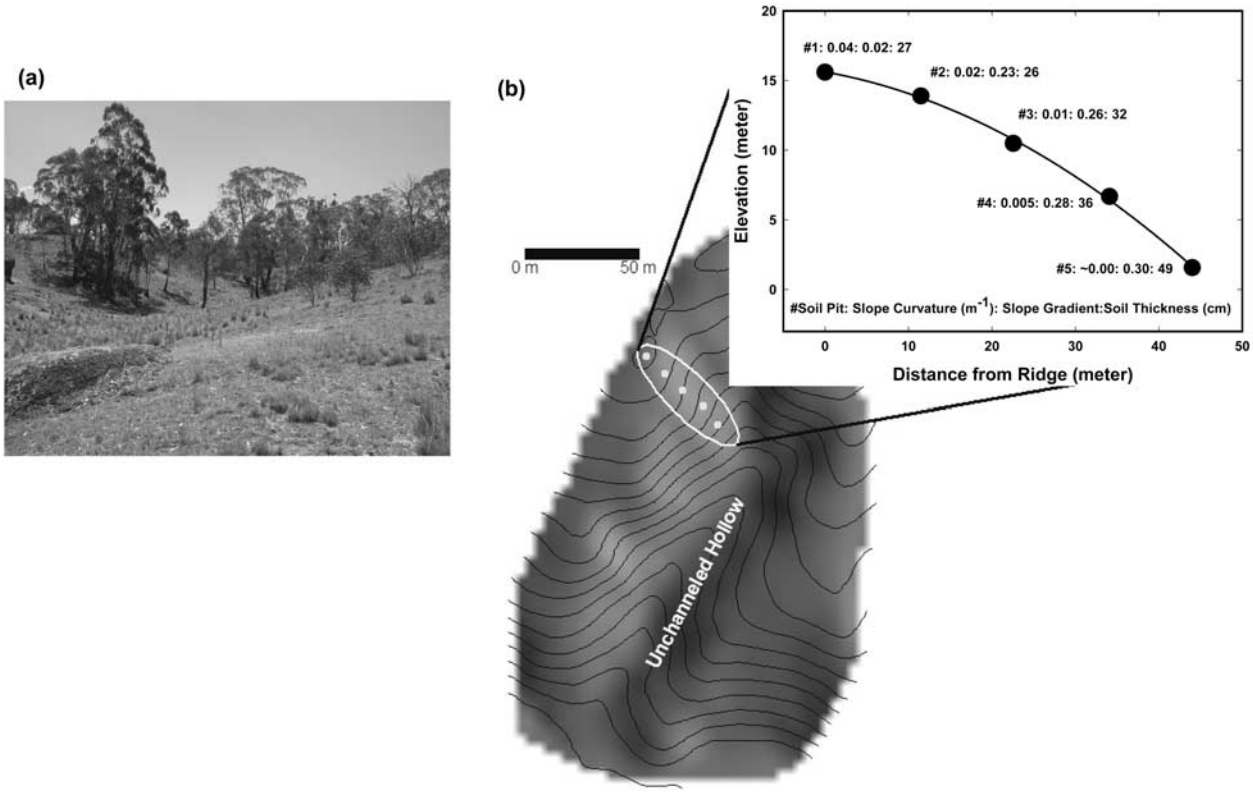

Figure 2. (a) Photograph of the Frog's Hollow zero-order watershed looking north and (b) planar and cross-section view of the transect showing excavated soil pits. The numbers beside the points on the cross section in Figure 2b represent soil pit number, negative curvature (m^{-1}), slope gradient (unitless), and soil thickness (cm), respectively.

about 80 km south–southeast from Canberra, New South Wales, Australia (Figure 2a) [*Heimsath et al.*, 2001]. The site is located 75 km inland from the coast, at an elevation of 930 m, and is part of a rolling highland. The highland is separated from the lower coastal belt by a steep escarpment, 12 km from the study site, formed during the Cretaceous Australian continental rift [e.g., *Seidl et al.*, 1996]. The bedrock is the Anembo granodiorite [*Richardson*, 1976], and the land surface is dotted with weathering resistant tors. The mean annual precipitation ranges between 550 and 750 mm, and the rainfall is evenly distributed through the year. Daily maximum (minimum) temperatures vary from 8 (−2) in winter to 23 (9) °C in summer (Bureau of Meteorology, Australian Government, Climate averages for Australia, 2002, available at http://www.bom.gov.au/climate/averages/).

[22] Soil transport is driven primarily by bioturbation, though overland flow may occur after fires [*Heimsath et al.*, 2001]. Ant mounds are widespread, and wombat burrows are concentrated in the lower slope areas and in unchanneled hollows where soils are thicker. Biological disruption of saprolite, such as animal burrowing and tree throw, leads to soil production [*Heimsath et al.*, 2001]. Including the studied catchment, *Heimsath et al.* [2005a] measured concentrations of in situ produced cosmogenic ^{10}Be and ^{26}Al in saprolite samples beneath the soil mantle to determine soil production rates across the landscape spanning the escarpment. They report a soil production function, $\Phi = \rho_r \Phi_o e^{-\alpha H}$ (where $\Phi_o = 53 \pm 2$ m Ma^{-1}, $\alpha = 0.022 \pm 0.001$ cm^{-1}, and H is slope normal soil thickness in cm) to quantify soil production rates for eroding soil mantled landscapes such as the one studied here. We use this well-defined soil production function in our model calculations.

[23] Soil characteristics across the landscape support the assumption that they are at steady state. First, abrupt soil horizon boundaries or buried A horizons were absent on both the convex slope and in the adjacent depositional hollow, indicating continuous erosion/deposition from the slope. Second, the intense vertical soil mixing suggests that the soil mantle is steadily removed and replaced by soil transport and soil production. The hypothesis of gradual and continuous soil erosion is supported by *Heimsath et al.* [2001], who suggested that the last event of climatic and erosional perturbation had occurred 150 ka ago at the site. Their modeling work also suggested that the soils in the catchment have been replaced multiple times and reached steady state since the last major erosional perturbation. Lastly, aeolian dust inputs are unlikely to be significant in terms of soil mass balance: Soil samples from the summit and base had zircon grains with sharp euhedral morphologies derived from underlying bedrock and did not include rounded aeolian zircons [*Brimhall et al.*, 1993]. The possibility of zircon-depleted aeolian inputs is also unlikely given the high Zr concentration of aeolian soils in the region [*Dickson and Scott*, 1998].

4.2. Sampling and Analysis

[24] We excavated five soil pits at the summit, shoulder, and backslope positions [*Ruhe and Walker*, 1968] along

Table 1. Morphological Descriptions of Soils, Bulk Densities, and Rock Fragment Content[a]

Soil	Horizon	Depth, Cm	Horizon Boundary[b]	Color (Dry)	Structure[c]	Roots[d]	Pores[d]	Clay Film[e]
1	A1	0–6	C,S	10YR3/2	1, m, sbk	2f, 2vf	1m	NE[f]
	A2	6–15	C,S	10YR3/2	1, m and c, sbk	2f, 2vf	2m, 1f	NE
	Bw	15–27	C,S	10YR7/2	3, c, sbk	1f	1f	NE
	Sap	27–47			M[g]	1f, 1vf	1c	Red stains
2	A1	0–5	C,S	10YR5/2	1, s and m, sbk	2f, 2vf	1m	NE
	A2	5–10	C,S	10YR6/3	1, s, sbk	2f, 2vf	2m, 1f	NE
	Bw	10–26	C,S	10YR7/2	1, s and m, sbk	1f	1f	NE
	Sap	26–45			M	NE	1c	1–3, pf
3	A1	0–5	C,S	10YR6/2	2, m and c, sbk	1f, 2vf	1m, 1f	NE
	A2	6–15	G,S	10YR7/3	2, m and c, sbk	1f, 2vf	1m, 1f	NE
	Bw	15–32	C,S	10YR7/2	2, m and c, sbk	2vf	2f	NE
	Sap	32–50			M	1f,1vf	NE	NE
4	A1	0–2	C,S	10YR6/3	2, m, sbk	1vf	1f	NE
	A2	2–15	G,S	10YR7/3	2, m and c, sbk	1vf	1vf	NE
	Bw	15–36	C,I	10YR7/3	2, m and c, sbk	1c, 1m,1f, 1vf	1c, 1m, 1f, 1vf	NE
	Sap	36–60			M	1c, 1vf	1c, 1vf	pf
5	A1	0–5	C,S	10YR3/2[h]	2, f and m, sbk	1m	2c, 1f, 2vf	NE
	A2	5–21	G,S	10YR3/3	2, m and c, sbk	1c, 1m, 1f, 1vf	1m, 1f	NE
	AB	21–32	G,S	10YR4/4	2, m and c, sbk	1c, 1f, 1vf	1c, 1f	NE
	Bw	32–49	C,S	10YR4/4	2, m and c, sbk	1c, 1m, 1f	1c, 1f	NE
	Sap	49–67			M	1m, 1f	NE	pf

[a]No spatial trend was observed for the saprolite and soil bulk densities. The averaged saprolite bulk density is 1.8 ± 0.1 g cm^{-3} (N = 5). Soil bulk densities varied with depth: 1.2 ± 0.06 g cm^{-3} for A1 horizons (N = 9), 1.5 ± 0.04 g cm^{-3} for A2, A3, AB, and BA horizons (N = 12), 1.7 ± 0.03 g cm^{-3} for Bw horizons (N = 10). The rock content with depth was: 22 ± 2.4% for A1 horizons (N = 10), 28 ± 2.6 for A2, A3, AB, and BA horizons (N = 11), and 36 ± 4.3% for Bw horizons (N = 11).

[b]C: clear, S: smooth, G: gradual, I: irregular.

[c]1: weak, 2: moderate, 3: strong, m: medium, c: coarse, f: fine, sbk: subangular blocky.

[d]1: few (<1/cm^2 for very fine and fine, <1/dm^2 for medium and coarse), 2: common (1–5/cm^2 for very fine and fine, 1–5/dm^2 for medium and coarse), vf: very fine (<1 mm diameter), f: fine (1–2 mm diameter), m: medium (2–5 mm diameter), c: coarse (5–10 mm diameter).

[e]p: patchy, f: faint.

[f]NE: nonexistant.

[g]M: massive.

[h]The darker colors (lower values) of soil 5 are due to their higher organic carbon content.

a ~50-m-long slope where exposed tors are absent (Figure 2b). All sites were on the convex segment of the hillslope, above the concave depositional hollow. Care was taken to ensure that soils were sampled along a water flow line. Additionally, two soil pits were excavated in the hollow axis to better constrain the soil erosion history. We used an existing survey of the hillslope [*Heimsath et al.*, 2001] in choosing a slope transect with minimal plan curvature. The ratios of contour lengths (equation (10)) were roughly 0.7 near the hillslope ridge but generally between 0.95 and 1 along the rest of the transect, indicating the decreasing horizontal convexity in the downslope direction.

[25] Soils were excavated to a depth of >20 cm below the soil-saprolite boundary in order to clearly identify the boundary. The soil thicknesses were later used to estimate soil production rates using the depth-dependent soil production function established for the soil mantled hillslopes in the area [*Heimsath et al.*, 2005a]. Samples and bulk density cores were collected in each soil horizon and saprolite. Bulk density cores (diameter of 5 cm and length of 15 cm) were oven dried at 110°C for a day and then weighed. Morphological descriptions of the excavated soils are shown in Table 1. Soils are characterized by thin A horizons and weakly developed Bw horizons, reflecting a combination of the semiarid conditions and active soil mixing and transport. We classified the soils as coarse-loamy to sandy skeletal Lithic Ustorthents.

[26] Rock fragments (>2 mm) were sieved from the soil and weighed. Splits of sieved samples were ground in a tungsten carbide mortar, and elemental compositions were measured for both fine and rock fractions of soils and saprolite using ICP-MS and ICP-AES, following lithium borate fusion, at the ALS Chemex chemical laboratory (http://www.alschemex.com). To verify the validity of Zr as an immobile index element, we separated zircon grains from soils and saprolite at both the ridge and hollow using density and magnetic separations, and microscopically examined the collected grains. We measured the clay content of the fine earth (<2 mm) fraction. This fraction was first treated with hydrogen peroxide to remove organic matter, and then with sodium hexameta phosphate (and shaking) to disperse clays. About 40 g of the treated samples were analyzed for particle size distribution using the hydrometer method [*Day*, 1965].

[27] In addition to soil production rates, the models also require soil profile integrated elemental chemistry (C) for each site, which was calculated using the following equation:

$$C = \frac{\sum_{n=1}^{N} \rho_n \Delta h_n \left[f_n C_{n,>2mm} + (1 - f_n) C_{n,<2mm} \right]}{\sum_{n=1}^{N} \rho_n \Delta h_n}, \qquad (22)$$

where N is the total number of soil horizons, Δh is horizon thickness [L], f is the mass fraction of rock fragments [M M^{-1}], and the subscript n represents the nth soil horizon. The standard error of bulk density and rock fragment measurements were propagated into the integrated elemental concentrations.

[28] As mentioned earlier in the model development, on the basis of the bulk soil elemental chemistry and soil production rate, both soil chemical weathering rate and soil flux are simultaneously calculated using a numerical

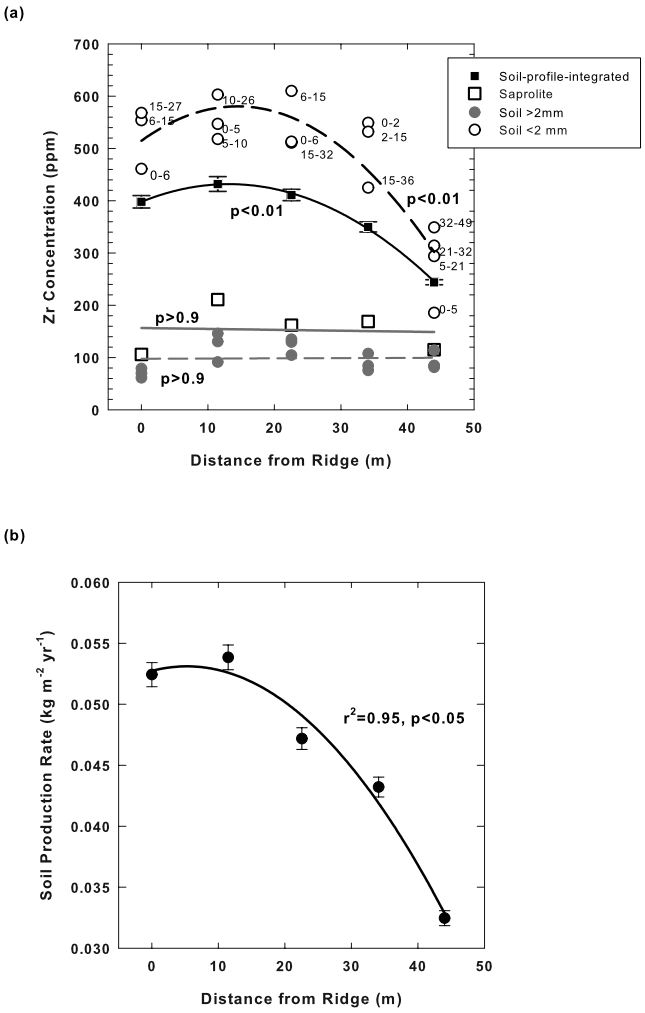

Figure 3. Model input variables used to calculate weathering rates and sediment fluxes. (a) Zr concentrations of soil and saprolite. Numbers adjacent to the <2 mm fraction data represent the sample horizon depths in cm. The error bars of the soil profile integrated values are calculated by propagating the standard errors in soil bulk density and the rock fragment fractions. The best fit polynomial line is $y = -0.211x^2 + 5.5796x + 397.11$ with $r^2 = 0.99$, which is subsequently used for calculating soil chemical weathering rate using equations (8) and (9) and (b) soil production rates calculated by combining the measured soil thickness and saprolite bulk densities with the published soil production function for the soil-covered hillslopes in the area [*Heimsath et al.*, 2005a]. The fitted line is $y = -0.0135x^2 + 0.1426x + 52.351$ with $r^2 = 0.98$.

iteration method. This process is essentially an inverse modeling which attributes the observed soil chemistry and thickness distributions that cannot be explained by physical processes of soil production and soil transport to soil chemical weathering.

5. Results and Discussion

5.1. Raw Data

[29] The profile-weighted soil Zr concentrations, [Zr], are higher than those of saprolite and decrease in the downslope direction (Figure 3a). The topographic variation of soil [Zr] is greater than the within-profile variation and that of saprolite [Zr]. Since the variation in saprolite [Zr] is less than that of soils and the soils represent the mixture of materials from saprolite and soil transported from upslope positions, the averaged saprolite [Zr] (148 ± 16 ppm N = 6) was used in our analyses. We note that this simplification does not lead to significant differences in results because of (1) a decreasing soil production rate in the downslope direction (Figure 3b), (2) larger [Zr] variation in soil than in saprolite, and (3) increasing amount of soil transported from upslope in downslope direction in contrast to the decreasing soil production rate. The soil Zr enrichments and the topographic variation of soil [Zr] were largely driven by the fine soil fraction (<2 mm), while rock fragments (>2 mm) are depleted in [Zr] relative to parent material. Profile integrated bulk soil Zr concentrations (equation (22)) were used in calculating chemical weathering rates.

[30] Soil thickness increased from 27 cm at the ridge to 49 cm in the downslope direction (Figure 2b). On the basis of the published soil production function [*Heimsath et al.*, 2005a] and the measured saprolite bulk densities at the site, the soil mass production rate decreases from ~0.050 to 0.03 kg m^{-2} yr^{-1} over the transect (Figure 3b). No topographic trends were found for the saprolite and soil bulk densities.

[31] Slightly different approaches were taken to calculate the total soil chemical weathering rate (equation (8)) versus individual element weathering rates (equation (9)). For the total soil weathering rate and soil flux rate, we used the fitted relationships between the distance from the ridge and the input variables: soil [Zr] and soil production rate. For individual element chemical weathering rates (equation (9)), we used the measured concentrations of those elements in local soils and saprolite because the spatial distribution of these concentrations, with the exception of [Zr], could not be well described with equations (Table 2). The soil flux determined with total chemical weathering rate was used in calculating the individual elemental weathering rates. The chemical weathering rates of individual elements, which require information on the gradient in soil chemistry, could thus be calculated only for the area between neighboring soil pits.

5.2. Soil Chemical Weathering Rates

5.2.1. Results

[32] The total soil chemical weathering rate decreases from a *loss* of 0.035 kg m^{-2} yr^{-1} at the ridge, to a *gain* of 0.035 kg m^{-2} yr^{-1} at the lowest end of the transect (Figure 4). The shift from loss to gain occurs between soils 4 and 5. The slope-averaged net weathering rate is a loss of 0.021 kg m^{-2} yr^{-1}. A mass of 1.0 kg yr^{-1} is annually leached from the soils on the upper part of the hillslope (across a 1 m length of contour line), and a mass of 0.1 kg yr^{-1} precipitates in some form in the soil at the base of the hillslope.

[33] We separately determined the contributions of W_Φ and W_S to the total chemical weathering rate (equation (8)) in order to illustrate the significance of the new term, W_S, that has not been previously accounted for in hillslope soil weathering studies. W_Φ, which was measured in *Riebe et al.* [2001, 2003a, 2003b, 2004], is always a net loss (Figure 4),

Table 2. Elemental Concentrations of Soils and Saprolite[a]

Soil (Distance From Ridge, m)	Depth, cm	LOI, %		Zr, ppm		Si, %		P,[b] %		Fe, %		Al, %		Ca, %		Mg, %		Na, %		K, %	
		F[c]	R[d]	F	R	F	R	F	R	F	R	F	R	F	R	F	R	F	R	F	R
1 (0)	0–6	4.98	1.04	461	61	35.2	41.3	0.009	-	0.95	0.52	4.93	2.22	0.76	0.24	0.070	0.020	0.77	0.39	3.84	1.73
	6–15	2.39	0.57	554	70	35.5	41.4	*0.002*	-	1.14	0.38	5.42	2.57	0.87	0.15	0.080	0.010	0.88	0.48	3.90	2.20
	15–27	1.58	0.52	568	79	35.8	41.4	0.004	-	1.19	0.38	5.77	2.48	0.86	0.20	0.080	0.020	0.93	0.42	4.05	1.97
	Sap	NA		106		38.1		0.0131		1.40		6.40		0.36		0.30		0.89		3.24	
2 (11.5)	0–5	4.2	1.22	547	146	35.5	41.5	0.022	-	1.04	0.46	4.92	2.13	0.65	0.03	0.072	0.024	0.82	0.35	3.64	1.74
	5–10	3.22	0.61	518	91	35.9	42.2	0.017	0.013	1.11	0.46	4.81	1.77	0.65	0.02	0.072	0.036	0.76	0.27	3.56	1.48
	10–26	1.61	0.66	603	131	36.0	41.1	0.009	-	1.31	0.59	5.40	2.46	0.75	0.01	0.072	0.024	0.89	0.44	3.78	1.86
	Sap	NA		211		38.1		0.017		1.81		6.67		0.52		0.36		0.82		3.16	
3 (22.6)	0–5	3.59	0.81	511	105	36.1	42.5	0.013	-	1.05	0.43	4.57	1.67	0.63	0.19	0.066	0.018	0.62	0.27	3.52	1.32
	6–15	2.31	0.92	610	130	36.2	41.4	0.013	-	1.18	0.54	4.93	2.27	0.69	0.26	0.066	0.024	0.69	0.40	3.58	1.59
	15–32	2.11	0.88	511	135	36.7	42.1	0.013	0.004	1.27	0.52	5.37	2.45	0.73	0.31	0.084	0.030	0.73	0.38	3.70	1.63
	Sap	NA		162		34.9		0.022		2.62		8.47		1.18		0.54		1.63		2.49	
4 (34.1)	0–2	4.04	0.72	549	75	34.1	41.2	0.017	0.017	1.94	0.43	5.72	2.91	1.01	0.58	0.217	0.036	1.02	0.73	3.40	1.30
	2–15	3.12	1.2	532	84	33.1	37.0	0.013	0.017	2.26	0.76	6.35	5.37	1.11	1.17	0.259	0.072	1.10	1.51	3.35	2.13
	15–36	3.01	1.38	425	108	32.5	36.3	0.013	0.004	2.62	1.01	7.01	5.98	1.16	1.24	0.368	0.121	1.19	1.52	3.51	2.32
	Sap	NA		169		34.9		0.035		3.02		7.78		1.55		0.78		1.86		2.57	
5 (44.0)	0–5	18.1	1.6	186	84	26.4	36.2	0.065	0.039	2.45	0.64	5.90	6.59	1.69	1.54	0.428	0.078	1.14	1.94	2.75	2.19
	5–21	7.51	1.82	294	81	30.3	35.9	0.061	0.032	3.11	0.83	7.28	5.82	1.63	1.33	0.501	0.109	1.36	1.68	3.22	2.00
	21–32	5.54	1.29	314	85	29.9	35.0	0.057	0.022	3.46	1.01	7.59	6.48	1.59	1.42	0.555	0.133	1.38	1.85	3.05	2.17
	32–49	5.12	1.86	349	114	29.5	36.7	0.061	*0.002*	3.70	1.17	8.02	5.29	1.54	1.08	0.603	0.163	1.37	1.36	3.08	1.85
	Sap	NA		115		33.1		0.044		1.82		8.05		1.90		0.32		2.15		2.50	

[a]NA: not available.

[b]Some soil samples had phosphorous contents (italicized) below the detection limit of ICP AES (P_2O_5 of less than 0.01%). For those soils, we used a value of 0.005% as the P_2O_5 content. To examine the effect of this assumption in calculations discussed in the text, we repeated calculations assuming values of 0.00 and 0.01%, but found little difference between the values chosen.

[c]F: fine fraction (<2 mm).

[d]R; rock fraction (>2 mm).

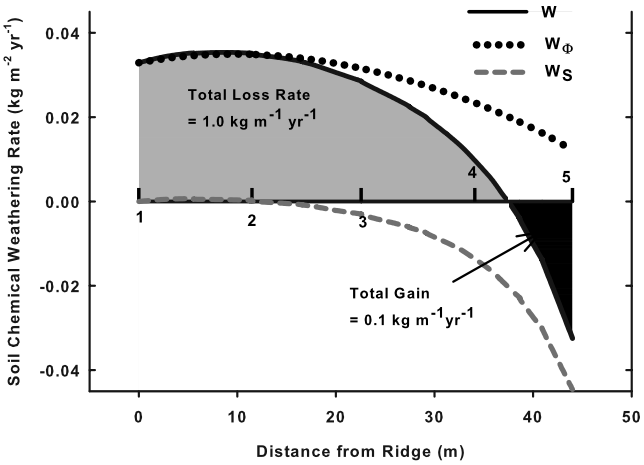

Figure 4. Calculated total soil chemical weathering rate per land surface area as a function of topographic position and the various components of the total soil chemical weathering rate per land surface area: W_Φ (dotted line) and W_S (dashed line) weathering rates constitute the total soil chemical weathering rate (solid line). Positive values indicate the mass loss from soil, and negative values represent a mass gain.

and decreases from 0.035 to 0.012 kg m^{-2} yr^{-1} down the hillslope, with a slope-averaged loss of 0.029 kg m^{-2} yr^{-1}. W_S however, is negligible near the summit, but results in increasing *gains* of up to 0.045 kg m^{-2} yr^{-1} in the downslope direction. When integrated over the hillslope, W_S shows a gain of 0.008 kg m^{-2} yr^{-1}. The addition of W_S to W_Φ ultimately shifts the total local weathering rates from a net loss to gain in some of the soils. The slope-averaged total weathering rate is 0.021 kg m^{-2} yr^{-1}, nearly 30% lower than the estimate derived solely by W_Φ.

[34] The calculated weathering rates of individual elements (Figure 5) revealed three trends. First, the net loss of the most abundant oxide elements (Si, Al, and Fe) consistently decreased in the downslope direction (Figure 5a). Second, the weathering rates of the major cations (Mg, Na, Ca, and K) were largest between sites 2 and 3, and they generally decreased in the downslope direction. Third, the apparent accumulation rates of P and Ca in soil at the base of the hillslope are comparable to their loss rates on the upper part of the slope (Figures 5b and 5c). When integrated over the entire transect, the P and Ca accumulation rates approach 85 and 25% of their loss rates, respectively.

[35] The contribution of chemical weathering to total soil mass removal systematically varies within the hillslope (Figure 6). The ECDF is greatest on the ridge where weathering removes nearly ~60% of the soil mass produced from bedrock. At the lower end of the hillslope (where soils are thicker, soil production rates lower, and lateral transport is very high), the apparent precipitation/deposition of solutes is as large as the soil production rate, and the ECDF is therefore close to −1. We note that the ECDF is equal to the CDF only near the ridge, and increasingly diverges from the CDF in the downslope direction. The CDF and ECDF differ greatly even when integrated for the entire hillslope. The spatially integrated ECDF is 0.4, while the integrated CDF is 0.6, which is 50% larger than the ECDF.

5.2.2. Discussion

[36] If soil chemical weathering rates were calculated solely on the soil elemental composition and the soil production rates, the hillslope-averaged weathering loss rate, and its contribution to mass removal, would have been

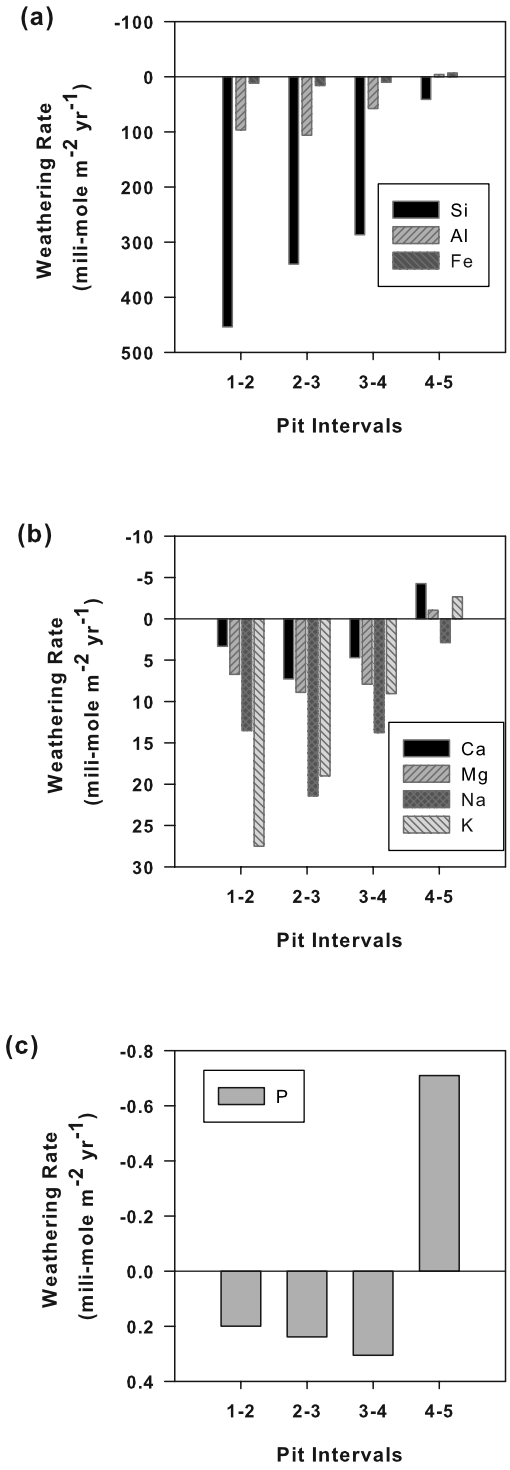

Figure 5. Weathering rates per land surface area of (a) most abundant oxide elements, (b) major cations, and (c) phosphorous. Positive values indicate a mass loss from soil while negative values represent a mass gain. Pit intervals represent the area between two neighboring soil pits.

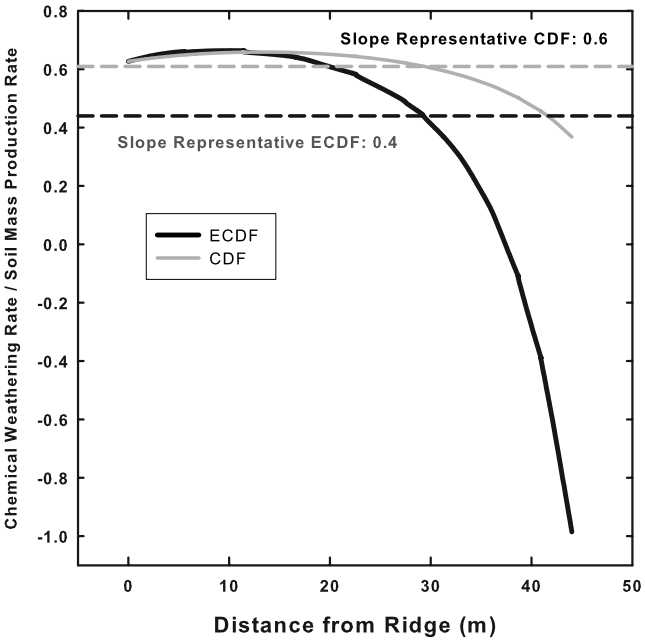

Figure 6. The ratio of the total soil chemical weathering rate to the soil mass production rate. The black solid line represents the extended chemical depletion factor (ECDF), and the gray solid line indicates the chemical depletion factor (CDF). The slope-averaged ECDF and CDF values are represented in the dashed black and gray lines, respectively.

overestimated by 40 and 50%, respectively, at our study site.

[37] The chemical weathering losses are dominated by Si and Al followed by K, Na, Fe, and Mg (Figures 5a and 5b). This calculation suggests that K-feldspars, Na plagioclases, and biotite (and possibly hornblende) are the major targets of chemical weathering. The XRD analyses of the soils from the pit 1 and 5 showed that 23% of the soil mass is composed of K-feldspar. While upslope soils are dominated by the mass losses via soil erosion and chemical weathering, there is a deposition of mass at the hillslope base whose mechanisms are not entirely understood. In the area between pit 4 and 5, the precipitation of Al and Fe, in contrast to the weathering loss of Si, (Figure 5a), suggests the precipitation of clay minerals.

[38] Several observations provide support to the clay precipitation. First, soils at the hillslope base have more clay than upslope soils. In addition to the clay (Table 3), soil elemental chemistry is also suggestive of higher clay contents in the lower soils. Compared to primary minerals, secondary minerals have lower ratios of Si to Al. The measured ratios of Si to Al in soils are 6.6 (soil 1), 7.1 (soil 2), 7.3 (soil 3), 5.2 (soil 4), and 4.0 (soil 5), reflecting the higher clay contents at the two soils at the hillslope base. If the higher clay contents in the soils 4 and 5 are due to more intense in situ weathering of primary minerals, those soils should show the greatest soil Zr enrichment. Instead, we found an opposite trend that soil [Zr] decreases in the downslope direction (Figure 3a). Given that clay fractions of granitic soils are most depleted in Zr [*Taboada et al.*, 2006], this discrepancy supports the hypothesis that Zr-depleted clay has been either translocated to the soils at the hillslope base or formed from lateral subsurface solute fluxes. Lateral translocation of clay in soils via water flow has been long considered as partly responsible for systematic variation of soil properties along hillslopes [*Hugget*, 1976; *Sommer and Schlichting*, 1997].

[39] The redistribution of mass downslope appears to be consistent with the groundwater hydrology at the site. On a hillslope summit roughly 100 m from our slope transect, the water table was at 9 m depth during June 2003 (B. Burke, unpublished data, 2003). If this water table is general for the area, the ground water table below the our summit position would be at a higher elevation than soils 4 and 5. While the water table should follow the topography, lateral gradients of water potential may generate ground water seepage through saprolite to the soils on lower slope. The saprolite is highly fractured on the basis of road cut observations, which should facilitate groundwater seepage. While the subsurface water flow pathways within the catchment are unknown, the particularly greater soil organic matter content at soil 5 is highly suggestive of an additional water source. The soil surface (0–5 cm) at site 5 had 7% carbon, which is much greater than the 1.1 to 1.8% carbon (N = 5) found in the other soils upslope. Additionally, the carbon to nitrogen ratios of the organic matter in soil 5 ranged from 14 (Bw) to 21 (A1), higher than ratios in the up-slope soils: 12 (Bw) to 17 (A1). C/N ratios decline as plant material undergoes microbial decomposition, and the increase in these ratios indicates enhanced plant production relative to decomposition that can only be driven by increased water availability in this semi arid climate.

[40] Another indication of lateral redistribution of mass is the topographic patterns of individual elements. The high abundance of K-feldspar explains why the calculated chemical weathering rate of K is the greatest among cations (Figure 5b). Between pit 4 and 5, however, the apparent higher precipitation rate of the biologically significant Ca is notable. In addition to Ca, a significant retention of the biologically important P is evident. The role of biology on the elemental redistribution along the hillslope is consistent with field observations of plant cover, and especially the soil organic matter measurements discussed above. Thus greater plant production and the corresponding incorporation of Ca and P, may partly contribute to the higher concentration of inorganic nutrients at the hillslope base.

[41] The soil chemical weathering rate is the divergence of solute flux (equations (8) and (9)). Solute gains and

Table 3. Measured Clay Content in the Fine Fraction of Soils at Slope Summit and Base[a]

Horizon	Soil 1	Soil 5
A1	16	20
A2	16	28
AB	no AB horizon	25
Clay mass per area, kg m^{-2}	25 kg m^{-2}	87 kg m^{-2}

[a]Clay contents were not measured for Bw horizons where visual and hand observation indicates low clay contents. Clay content is given in percent.

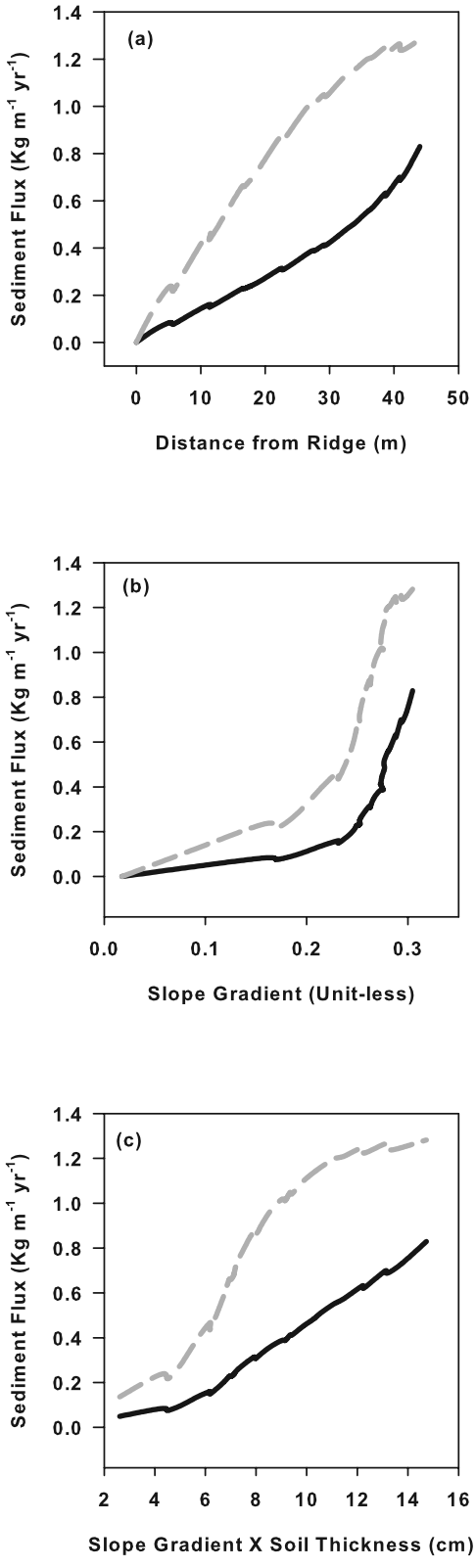

Figure 7. Calculated soil transport relative to (a) the distance from the ridge, (b) the slope gradient, and (c) the product of slope gradient and soil thickness. Solid lines indicate soil transport rates calculated after incorporating chemical weathering, and the gray dashed lines represent the soil transport in the case where no soil chemical weathering is assumed.

losses may be a function of the three dimensional distribution of water potentials, solute concentrations of mobile component j, sorption and desorption of dissolved ions onto the bedrock and soil media, and hydraulic conductivities. The measured saprolite bulk densities are 1.8 g cm^{-3}, only 70% of fresh granodiorite, indicating that significant dissolution and removal of weathering products has also occurred during saprolite formation. For example, the greater abundance of K (presumably from K-feldspar) than Ca in the soils (Table 2) indicates that more weatherable and abundant Ca-bearing plagioclases in granodiorite bedrock have been chemically weathered during the saprolite formation. Given the likelihood that solute fluxes may redistribute the weathering products from soil to saprolite and vice versa, our mass balance analysis, confined to the soil layer, are incomplete in accounting for the entire set of mass fluxes within a hillslope. Our model, however, does provide a solute flux term that captures the net result of all of these unidentified fluxes and offers an opportunity to ultimately couple hydrology to the topography-dependent chemical weathering rates.

[42] At Frogs Hollow, the CDF overestimates the contribution of chemical weathering to mass removal. The reason for this discrepancy is the fact that the 'parent material' of soils in the lower slope includes increasingly more preweathered soil material eroded from upslope positions. However, there may also be hillslopes where the CDF underestimates chemical weathering. Depending on the environmental conditions, soils at a hillslope base may be more enriched in immobile elements than the soils in the upper hillslope. This positive gradient of immobile element concentrations, when combined with soil transport at the site, will result in a positive (mass loss) W_S in equations (8) and (9). In this case, the CDF underestimates the actual contribution of soil chemical weathering to mass removal. Thus soil transport, depending on its magnitude, has the potential to significantly affect the calculation of catchment-scale weathering rates in various settings.

[43] One might question our assumption of negligible aeolian input. Earlier we mentioned the observed euhedral morphology of zircons in the soils and the generally high [Zr] of aeolian sands in the region, but we can further explore a hypothetical case where the soil [Zr] decreases downslope mainly because of the inputs of Zr-depleted aeolian dust. This scenario, however, appears unlikely. The soil [Zr] gradient was observed to be steeper in the downslope area where the soil flux is fastest, which can be only maintained by a nonlinearly increasing deposition rate of Zr-depleted aeolian dust in the downslope direction where the slope gradient is also steepest. Thus while we cannot completely reject the presence of aeolian deposition, it appears to be reasonable to assume that chemical weathering largely explains the observed pattern of soil [Zr].

5.3. Soil Transport Rates

[44] As described in the model development, we combined equations (8) and (10) using an iterative process to solve for the rates of soil transport and chemical weathering. The calculated soil flux (Q_s) increases in the downslope direction from zero at the ridge position (a model assumption) to ~0.8 kg m^{-1} yr^{-1} at the hillslope base (Figure 7a). The rate of physical soil transport, when calculated without

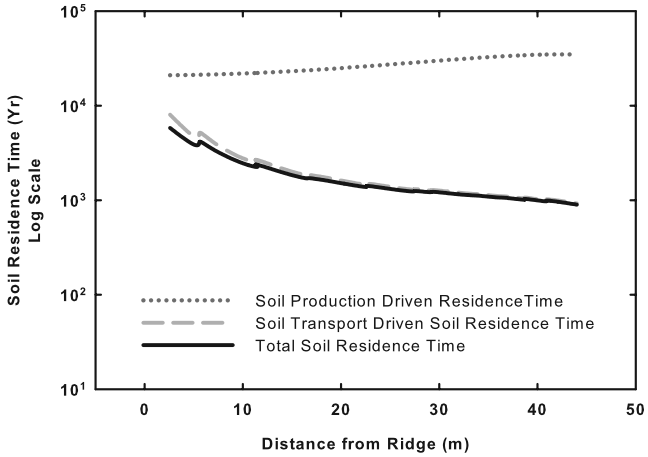

Figure 8. Calculated soil residence times along the hillslope transect. Total soil residence time is close to soil transport-driven soil residence time.

including the soil chemical weathering rate, was ~1.3 kg m^{-1} yr^{-1} at the hillslope base, a value 60% higher than that calculated including chemical mass loss. Thus the mass loss by chemical weathering will greatly affect hillslope evolution models where soil mass has commonly been assumed to be entirely due to physical transport (for review of soil transport models, see *Dietrich et al.* [2003]).

[45] Earlier, we calculated that the chemical weathering flux integrated over the hillslope is 0.9 kg m^{-1} yr^{-1}, which removes 40% (or less than half) of the total hillslope soil production. This disagrees with the calculated sediment flux of ~0.8 kg m^{-1} yr^{-1} for the hillslope base. The discrepancy does not indicate a fundamental error in our mass balance model. Instead, the discrepancy develops because we did not account for the horizontal divergence of solute flux ($\tilde{Q}_w$ in equation (8)) while factoring the diverging soil transport (equation (10)). This inconsistency in treating the fluxes of solute and soil resulted in slightly overestimating the weathering flux. To estimate the error by ignoring the horizontal divergence of solute flux, we calculated the rates of soil chemical weathering and soil transport for a hypothetical situation where horizontal convexity does not exist, while holding other model conditions constants. In this case, the soil chemical weathering integrated over the transect is reduced to 0.73 kg m^{-1} yr^{-1}, which is now less than the calculated sediment flux at the hillslope base. This exercise, however, also shows that the soil chemical weathering rate calculation is not significantly affected by not incorporating the diverging solute flux.

[46] Our work here can be used to test the nature of the physical transport law that best describes our field area. To compare the two models of soil transport (equations (3) and (4)), we plotted the calculated sediment flux (Q_s) against the slope gradient and the product of soil thickness and slope gradient. The calculated soil transport increases nonlinearly above slope gradient of 0.23 (Figure 7b). While nonlinear soil transport may develop at steep hillslopes because of the combined effects of gravity and friction [*Roering et al.*,1999], the hillslope at Frogs Hollow appears too gentle (gradients of up to 0.29) for such mechanism. The nonlinear transport has been observed only for slopes steeper than ~0.4 in the Oregon Coast Range [*Roering et al.*, 1999].

[47] Instead, our result supports the hypothesis by *Ahnert* [1967] that soil transport increases with the product of soil depth and slope gradient (equation (4)). The calculated sediment flux was linearly proportional to the product of soil thickness and slope gradient (Figure 7c). Soil chemical weathering does not seem to be one of the causes for this trend. Soil transport, calculated assuming no soil chemical weathering, still exhibits a linear relationship to the product of soil thickness and slope gradient (Figure 7c). At this point, we are hypothesizing that more and larger organisms participate in soil movement as soil thickens [*Yoo et al.*, 2005]. Indeed wombats, which are the major soil burrowing organism at the study site, habituate the soils at the base of hillslopes mantled with thicker soils. The derivation and implications of a soil thickness–dependent transport model has recently been examined by *Heimsath et al.* [2005b].

5.4. Residence Time

[48] Soil residence times, involving both soil production and lateral transport, were calculated for the Frog's Hollow transect (Figure 8). The portion of the net residence time due to soil production, $T_{R\uparrow}$, increases from 21 to 35 ka in the downslope direction largely because of decreasing soil production rates and increasing soil thicknesses. If soil mass, instead of Zr mass, was divided by the soil production rate, the resulting soil residence time would be about 10 ka. In contrast, the $T_{R\rightarrow}$ decreases from 5 to 0.9 ka in the downslope direction (Figure 8) reflecting the increasing soil transport that occurs downslope (Figure 7a). The total soil residence time decreases from 4 ka on the ridge, to 0.9 ka at the hillslope base (Figure 8). When the residence time is integrated from the ridge to the hillslope base, the result shows that it takes 60 ka for soil to travel from the ridge to the hillslope base.

[49] By combining the position-dependent soil chemical weathering rates (Figure 4) and residence times (Figure 8) with equation (21), we calculated that a packet of soil (defined as the volume of a column below 1 m^2 surface area) losses roughly 1,800 kg through chemical weathering while traveling downslope. However, this weathering loss does not lead to gradual soil Zr enrichment, because during the transport, 3100 kg of fresh minerals from the saprolite are added to the soil diluting soil [Zr], and Zr dilution is also caused by the precipitation of Zr-depleted materials at the hillslope base. As the soil moves through the chemical precipitation zone, the soil gains roughly 90 kg of mass, which is about the same as the increase in clay between the hillslope base and summit (62 kg) (Table 3). The similarity of these calculated and measured parameters provides support for the hypothesis that weathering derived solutes or products are partially redistributed across this hillslope.

[50] Soil residence time provides a unique dynamic perspective for studying hillslope soil formation. Soil turnover along the hillslope is largely driven by lateral soil transport rather than vertical soil production. Consequently, as long as soil transport rates increase in the downslope direction, the time in which the materials in a soil is exposed to the local chemical weathering at a specific topographic position will be the longest on the ridge and will become increasingly brief downslope. At Frog's Hollow, soil is most

enriched in Zr near the summit (Figure 3a) not only because of the highest chemical weathering mass loss rate (Figure 4) but also because of the longest soil residence time (Figure 8). As that soil migrates downslope, in addition to picking up fresh minerals from saprolite, it passes through the zones of lower chemical loss rates, and net accumulation, with increasingly shorter residence times. The result is that the weathered, Zr-enriched soil material regains only a portion of its lost mass.

[51] Although 60 ka is required for the soil to travel the ~50 m distance from summit to the hillslope base, the observed soil profiles at all hillslope positions are similar in terms of horizon development (Table 1). Besides the small variations in soil properties along the transect, clay-rich B horizons, which would be expected in soils that have experienced as much as 60 ka of weathering, are absent along the entire hillslope. This appears to reflect that the soils are continuously replaced and mixed by soil inputs from upslope and by bioturbation. A soil with the volume of about 1 m^3 is replaced by soil production and soil transport in less than 5 ka at all positions along the hillslope transect (Figure 8), hindering soil profile development.

6. Conclusions

[52] Hillslope soils are a result of in situ bedrock conversion to soil, soil transport, and solute transport, all of which vary systematically with topographic position. The deconvolution of the magnitude and relative importance of these distinct trajectories can only be unraveled when a process-oriented soil transport model is integrated with a geochemical mass balance model. This approach yields perspectives that differ from simple intuitive expectations, and show that initial attempts by *Riebe et al.* [2001, 2003a, 2003b, 2004] to separate physical from chemical denudation of landscapes are very special cases of landscape evolution. Only through a combined evaluation of soil production and soil transport can the magnitude, spatial distribution, and even the sign, of chemical weathering be determined.

[53] When applied to a well-studied hillslope in Australia, we have found that over very short distances (~50 m), the net chemical weathering rate varies from positive (loss) to negative (gains) because of variations in sediment and solute fluxes. Additionally, the model provides us with a rigorous understanding of residence times on hillslopes, and shows that they vary by orders of magnitude over 50 m distances. These residence times, combined with the understanding that hillslope soil is derived from in situ parent material *and* the soil eroded from upslope, provide new insights into spatial patterns of soil morphological, physical, and chemical features.

Appendix A: Derivation of Equation (8)

[54] The following derivation of equation (8) also applies to equation (9). At steady state, the mass balance of bulk soil (equation (5)) becomes

$$\frac{\partial(\rho_s h)}{\partial t} = 0 = \Phi - \nabla \cdot \tilde{Q}_s - \nabla \cdot \tilde{Q}_w \tag{A1}$$

[55] At steady state, the mass balance of an immobile element (equation (7)) becomes

$$\begin{aligned}\frac{\partial(C_{is}\rho_s h)}{\partial t} &= 0 = C_{ip}\Phi - \nabla \cdot \left(C_{is}\tilde{Q}_s\right) \\ &= C_{ip}\Phi - \nabla C_{is} \cdot \tilde{Q}_s - C_{is}\nabla \cdot \tilde{Q}_s\end{aligned} \tag{A2}$$

If C_{is} is multiplied to equation (A1), then

$$C_{is}\Phi - C_{is}\nabla \cdot \tilde{Q}_s - C_{is}\nabla \cdot \tilde{Q}_w = 0 \tag{A3}$$

Subtracting equation (A3) from equation (A2) yields

$$\left(C_{ip} - C_{is}\right)\Phi - \nabla C_{is} \cdot \tilde{Q}_s + C_{is}\nabla \cdot \tilde{Q}_w = 0 \tag{A4}$$

[56] By rearranging equation (A4), we obtain the weathering rate model:

$$W = \nabla \cdot \tilde{Q}_w = \left(1 - C_{ip}/C_{is}\right)\Phi + \left(\nabla C_{is}/C_{is}\right) \cdot \tilde{Q}_s \tag{A5}$$

Appendix B: Derivation of Equation (13)

[57] If a mass of parent material with a bulk density of ρ_p and a thickness of h_p is converted to a soil with bulk density of ρ_s and thickness of h_s, then the mass of chemical weathering loss ($\Delta_\uparrow$) during the conversion is

$$\Delta_\uparrow = \rho_p h_p - \rho_s h_s. \tag{B1}$$

[58] Since the mass of an immobile element is conserved during the conversion, its mass conservation can be written as

$$C_{ip}\rho_p h_p = C_{is}\rho_s h_s. \tag{B2}$$

[59] Using equation (B2), $\Delta_\uparrow$ in equation (B1) can be rewritten as

$$\Delta_\uparrow = \left(\frac{C_{is}}{C_{ip}} - 1\right)\rho_s h_s. \tag{B3}$$

[60] **Acknowledgments.** We thank Benjamin Burke for his help in field work and providing some of saprolite bulk density data. We thank Simon M. Mudd for a review of an early version of this paper. We appreciate the thoughtful reviews by Editor R. S. Anderson and Associate Editor S. P. Anderson. This research was funded by National Science Foundation support to R.A. and A.H.

References

Ahnert, F. (1967), The role of equilibrium concept in the interpretation of landforms of fluvial erosion and deposition, in *L'evolution des Versants*, edited by P. Macar, pp. 23–41, Univ. of Liege, Liege, France.

Amundson, R. (2004), Soil formation, in *Treatise on Geochemistry*, edited by H. D. Holland and K. K. Turekian, pp. 1–35, Elsevier, New York.

Anderson, S. P., W. E. Dietrich, and G. H. Brimhall (2002), Weathering profiles, mass-balance analysis, and rates of solute loss: Linkages between weathering and erosion in a small, steep catchment, *GSA Bull.*, *114*(9), 1143–1158.

Andrews, D. J., and R. C. Bucknam (1987), Fitting degradation of shoreline scarps by a nonlinear diffusion model, *J. Geophys. Res.*, *92*(B12), 12,857–12,867.

Berner, E. K., and R. A. Berner (2004), Plants and mineral weathering: Present and past, in *Surface and Ground Water, Weathering, and Soils*, *Treatise on Geochemistry*, vol. 5, edited by J. I. Drever, pp. 169–188, Elsevier, New York.

Berner, R. A. (1995), Chemical weathering and its effect on atmospheric CO_2 and climate, in *Chemical Weathering Rates of Silicate Minerals*, edited by A. F. White and S. L. Brantley, pp. 565–583, Mineral. Soc. of Am., Washington, D. C.

Birkeland, P. W. (1999), *Soils and Geomorphology*, 430 pp., Oxford Univ. Press, New York.

Brantley, S. L., and Y. Chen (1995), Chemical weathering rates of pyroxenes and amphiboles, in *Chemical Weathering Rates of Silicate Minerals*, edited by A. F. White and S. L. Brantley, pp. 119–172, Mineral. Soc. of Am., Washington, D. C.

Braun, J., A. M. Heimsath, and J. Chappell (2001), Sediment transport mechanisms on soil-mantled hillslopes, *Geology*, *29*(8), 683–686.

Brimhall, G. H., and W. E. Dietrich (1987), Constitutive mass balance relations between chemical composition, volume, density, porosity, and strain in metasomatic hydrochemical systems: Results on weathering and pedogenesis, *Geochim. Cosmochim. Acta*, *51*, 567–587.

Brimhall, G. H., O. A. Chadwick, C. J. Lewis, W. Compston, I. S. Williams, K. J. Danti, W. E. Dietrich, M. E. Power, D. Hendricks, and J. Bratt (1991), Deformational mass transport and invasive processes in soil evolution, *Science*, *255*, 695–702.

Brimhall, G. H., W. Compston, I. S. Williams, R. F. Reinfrank, and C. J. Lewis (1993), Darwinian zircons as provenance tracers of dust-size exotic components in laterites: Mass balance and SHRIMP ion microprobe results, in *Soil Micromorphology: Studies in Management and Genesis*, edited by A. J. Ringrose-Voase and G. G. Humphreys, pp. 65–81, Elsevier, New York.

Chadwick, O. A., G. H. Brimhall, and D. M. Hendricks (1990), From a black to a gray box: A mass balance interpretation of pedogenesis, *Geomorphology*, *3*, 369–390.

Chadwick, O. A., L. A. Derry, P. M. Vitousek, B. J. Huebert, and L. O. Hedin (1999), Changing sources of nutrients during four million years of ecosystem development, *Nature*, *397*, 491–497.

Culling, W. E. H. (1963), Soil creep and the development of hillside slopes, *J. Geol.*, *71*(2), 127–161.

Day, P. R. (1965), Particle fractionation and particle-size analysis, in *Methods of Soil Analysis 1*, edited by C. A. Black, pp. 545–567, Am. Soc. of Agronomy, Madison, Wis.

Dickson, B. L., and K. M. Scott (1998), Recognition of aeolian soils of the Blayney district, NSW: Implications for mineral exploration, *J. Geochem. Res.*, *63*, 237–251.

Dietrich, W. E., R. Reiss, M. L. Hsu, and D. R. Montgomery (1995), A process-based model for colluvial soil depth and shallow landsliding using digital elevation data, *Hydrol. Processes*, *9*(3–4), 383–400.

Dietrich, W. E., D. G. Bellugi, L. S. Sklar, J. D. Stock, A. M. Heimsath, and J. J. Roering (2003), Geomorphic transport laws for predicting landscape form and dynamics, in *Predictions in Geomorphology*, edited by P. R. Wilcock and R. M. Iverson, pp. 103–132, AGU, Washington, D. C.

Drever, J. I. (1994), The effect of land plants on weathering rates of silicate minerals, *Geochim. Cosmochim. Acta*, *58*(10), 2325–2332.

Fernandes, N. F., and W. E. Dietrich (1997), Hillslope evolution by diffusive processes: The timescale for equilibrium adjustments, *Water Resour. Res.*, *33*(6), 1307–1318.

Furbish, D. J. (2003), Using the dynamically coupled behavior of land-surface geometry and soil thickness in developing and testing hillslope evolution models, in *Predictions in Geomorphology*, edited by P. R. Wilcock and R. M. Iverson, pp. 169–181, AGU, Washington, D. C.

Gilbert, G. K. (1909), The convexity of hilltops, *J. Geol.*, *17*, 344–350.

Heimsath, A. M., W. E. Dietrich, K. Nishiizumi, and R. C. Finkel (1997), The soil production function and landscape equilibrium, *Nature*, *388*, 358–361.

Heimsath, A. M., J. Chappell, W. E. Dietrich, K. Nishiizumi, and R. C. Finkel (2001), Late Quaternary erosion in southeastern Australia: A field example using cosmogenic nuclides, *Quat. Int.*, *83–85*, 169–185.

Heimsath, A. M., J. Chappell, K. Nishiizumi, R. C. Finkel, and K. Fifield (2005a), Escarpment erosion and landscape evolution in southeastern Australia, *Spec. Pap. Geol. Soc. Am.*, *398*, 173–190, doi:10.1130/2005.2398(10).

Heimsath, A. M., D. J. Furbish, and W. E. Dietrich (2005b), The illusion of diffusion: Field evidence for depth dependent sediment transport, *Geology*, *33*(12), 949–952.

Hugget, R. J. (1976), Lateral translocation of soil plasma through a small valley basin in the Northaw Great Wood, Hertfordshire, *Earth Surf. Processes Landforms*, *1*, 99–109.

Likens, G. E., and F. H. Bormann (1977), *Biogeochemistry of a Forested Ecosystem*, 159 pp., Springer, New York.

Merritts, D. J., O. A. Chadwick, and D. M. Hendricks (1991), Rates and processes of soil evolution on uplifted marine terraces, northern California, *Geoderma*, *51*, 241–275.

Mudd, S. M., and D. J. Furbish (2004), Influence of chemical denudation on hillslope morphology, *J. Geophys. Res.*, *109*, F02001, doi:10.1029/2003JF000087.

Nezat, C. A., J. D. Blum, A. Klaue, C. E. Johnson, and T. G. Siccama (2004), Influence of landscape positions and vegetation on long-term weathering rates at the Hubbard Brook Experimental Forest, New Hampshire, USA, *Geochem. Cosmochim. Acta*, *68*(14), 3065–3078.

Porder, S., A. Paytan, and P. M. Vitousek (2005), Erosion and landscape development affect plant nutrient status in the Hawaiian Islands, *Oecologia*, *142*, 440–449.

Richardson, S. J. (1976), Geology of the Michelago, sheet 8726, 1:100000, Geol. Surv. of N. S. W., Sydney, Australia.

Riebe, C., J. Kirchner, D. Granger, and R. Finkel (2001), Strong tectonic and weak climatic control of long-term chemical weathering rates, *Geology*, *29*(6), 511–514.

Riebe, C. S., J. W. Kirchner, and R. C. Finkel (2003a), Long-term rates of chemical weathering and physical erosion from cosmogenic nuclides and geochemical mass balance, *Geochem. Cosmochim. Acta*, *67*(22), 4411–4427.

Riebe, C. S., J. W. Kirchner, and R. C. Finkel (2003b), Sharp decrease in long-term chemical weathering rates along an altitudinal transect, *Earth Planet. Sci. Lett.*, *218*, 421–434.

Riebe, C. S., J. W. Kirchner, and R. C. Finkel (2004), Erosional and climatic effects on long-term chemical weathering rates in granitic landscapes spanning diverse climate regimes, *Earth Planet. Sci. Lett.*, *224*(3–4), 547–562.

Roering, J. J., J. W. Kirchner, and W. E. Dietrich (1999), Evidence for nonlinear, diffusive sediment transport on hillslopes and implications for landscape morphology, *Water Resour. Res.*, *35*(3), 853–870.

Roering, J. J., et al. (2001), Hillslope evolution by nonlinear, slope-dependent transport: Steady state morphology and equilibrium adjustment timescales, *J. Geophys. Res.*, *106*(B8), 16,499–16,513.

Ruhe, R. V., and P. H. Walker (1968), Hillslope models and soil formation: I. Open systems, *Transactions of the 9th International Congress on Soil Science*, vol. 4, pp. 551–560, Elsevier, New York.

Seidl, M. A., J. K. Weissel, and L. F. Pratson (1996), The kinematics and pattern of escarpment retreat across the rifted continental margin of SE Australia, *Basin Res.*, *12*, 301–316.

Sommer, M., and E. Schlichting (1997), Archetypes of catenas in respect to matter: A concept for structuring and grouping catenas, *Geoderma*, *76*, 1–33.

Taboada, T., A. M. Cortizas, C. García, and E. García-Rodega (2006), Particle-size fractionation of titanium and zirconium during weathering and pedogenesis of granitic rocks in NW Spain, *Geoderma*, *131*, 218–236.

White, A. F., and A. E. Blum (1995), Effects of climate on chemical weathering in watersheds, *Geochem. Cosmochim. Acta*, *59*, 1729–1747.

White, A. F., A. E. Blum, M. S. Schulz, T. D. Bullen, J. W. Harden, and M. L. Peterson (1996), Chemical weathering rates of a soil chronosequence on granitic alluvium: 1. Quantification of mineralogical and surface area changes and calculation of primary silicate reaction rates, *Geochem. Cosmochim. Acta*, *60*(14), 2533–2550.

Yoo, K., R. Amundson, A. M. Heimsath, and W. E. Dietrich (2005), A process based model linking pocket gopher (*Thomomys Bottae*) activity to sediment transport and soil thickness, *Geology*, *33*(11), 917–920.

R. Amundson, Division of Ecosystem Sciences, 137 Mulford Hall, University of California, Berkeley, CA 94720-3110, USA. (earthy@nature.berkeley.edu)

G. H. Brimhall and W. E. Dietrich, Department of Earth and Planetary Science, University of California, Berkeley, CA 94720, USA. (bill@geomorph.berkeley.edu; brimhall@eps.berkeley.edu)

A. M. Heimsath, Department of Earth Sciences, Dartmouth College, 6105 Fairchild Hall, Hanover, NH 08755, USA. (arjun.heimsath@dartmouth.edu)

K. Yoo, Plant and Soil Sciences Department, University of Delaware, Newark, DE 19716-2170, USA. (kyoo@udel.edu)